Nanoscale

PAPER

View Article Online
View Journal | View Issue

Cite this: *Nanoscale*, 2015, **7**, 17131

Neuron-like differentiation of mesenchymal stem cells on silicon nanowires†

Hyunju Kim,[a] Ilsoo Kim,[b] Heon-Jin Choi,[b] So Yeon Kim*[a,c] and Eun Gyeong Yang*[a,d]

Received 25th August 2015,
Accepted 11th September 2015

DOI: 10.1039/c5nr05787f

www.rsc.org/nanoscale

The behavior of mammalian cells on vertical nanowire (NW) arrays, including cell spreading and the dynamic distribution of focal adhesions and cytoskeletal proteins, has been intensively studied to extend the implications for cellular manipulations *in vitro*. Prompted by the result that cells on silicon (Si) NWs showed morphological changes and reduced migration rates, we have explored the transition of mesenchymal stem cells into a neuronal lineage by using SiNWs with varying lengths. When human mesenchymal stem cells (hMSCs) were cultured on the longest SiNWs for 3 days, most of the cells exhibited elongated shapes with neurite-like extensions and dot-like focal adhesions that were prominently observed along with actin filaments. Under these circumstances, the cell motility analyzed by live cell imaging was found to decrease due to the presence of SiNWs. In addition, the slowed growth rate, as well as the reduced population of S phase cells, suggested that the cell cycle was likely arrested in response to the differentiation process. Furthermore, we measured the mRNA levels of several lineage-specific markers to confirm that the SiNWs actually induced neuron-like differentiation of the hMSCs while hampering their osteogenic differentiation. Taken together, our results implied that SiNWs were capable of inducing active reorganization of cellular behaviors, collectively guiding the fate of hMSCs into the neural lineage even in the absence of any inducing reagent.

Introduction

The precise control of materials on the nanometer scale has facilitated the application of these nanomaterials in a variety of ways, from manipulating cell morphologies *in vitro* to developing implanted devices such as nanobiosensors or drug delivery devices *in vivo*.[1–5] Among such materials, silicon nanowires (SiNWs) have been attracting great interest due to their ability to penetrate through the cellular membrane for intracellular delivery and sensing, the ease with which they can be chemically modified to obtain controlled surface properties, their size being comparable to that of biomolecules, and their coverage of a wide range of conductances.[6–11] Similarly to other nanomaterials with unique physical and chemical properties (for reviews, see ref. 3 and 12), NWs can also play a supportive role in the lineage-specific differentiation of stem cells. For example, it has been reported that adjusted elasticity and enhanced cytoskeletal rearrangements mostly promote the differentiation of mesenchymal stem cells (MSCs) toward osteoblasts.[13,14] Biochemical details in correlation with the interactions between stem cells and nanostructures have recently been revealed to support osteoblast differentiation.[15–17]

Previously, we examined cell spreading and the adhesion behavior of HeLa cells and found that SiNWs actively organized adhesion-related molecules,[18] leading us to hypothesize that SiNWs with controlled physical properties may facilitate neuronal differentiation of stem cells. Supporting this hypothesis, a recent study reported neural differentiation of C3H10T1/2 cells on patterned Si nanopillars.[19] To further investigate this hypothesis, we chose to explore human mesenchymal stem cells (hMSCs). hMSCs intrinsically possess the ability to differentiate into osteocytes, chondrocytes, adipocytes, and myocytes, thus providing advantages in tissue engineering applications. In addition, their plasticity, low immunogenicity, and relatively low barriers with respect to ethical issues have allowed extensive exploration of their trans-differentiation into a variety of cells such as skin, liver and even brain cells like neuron and glia (for reviews, see ref. 20). In fact, tremendous efforts have been made to trans-differen-

[a]Center for Theragnosis, Biomedical Research Institute, Korea Institute of Science and Technology, Hwarangno 14-gil 5, Seongbuk-gu, Seoul 136-791, South Korea. E-mail: eunyang@kist.re.kr, soyeonkim@kist.re.kr; Fax: +82-2-958-5909; Tel: +82-2-958-5178, +82-2-958-5914
[b]Department of Materials Science and Engineering, Yonsei University, Seoul 120-749, South Korea
[c]Department of Biomedical Engineering, Korea University of Science and Technology, KIST campus, Seoul 136-791, South Korea
[d]Department of Biological Chemistry, Korea University of Science and Technology, KIST campus, Seoul 136-791, South Korea

†Electronic supplementary information (ESI) available. See DOI: 10.1039/c5nr05787f

tiate hMSCs into neurons for treating neurodegenerative diseases, using various supplements including proteins, cytokines and chemicals.[20–25] Furthermore, it has been shown that cytoskeletal tension or contraction and mechanical stimuli activated by mechanotransduction pathways actively reprogram the lineage commitment of hMSCs.[16,17,26–29]

In this study, we sought to investigate the cell spreading and morphological changes of hMSCs on SiNWs with varying lengths in the absence of any soluble differentiation factors. The distributions of cytoskeletal actin and the focal adhesion vinculin in neurite-like extensions as well as the cell motility were closely observed to assess their interactions with the surface. The growth rate, proliferation, and mRNA levels of neural-specific markers were measured to estimate possible neuronal differentiation. Our findings illustrated that physical stimulation by SiNWs could modulate cell adhesion behaviors, thereby promoting active reprogramming of hMSCs into the neural lineage.

Results and discussion

Physical properties and effects of NWs on morphological changes of hMSCs

To elucidate the mechanistic details of the morphological changes, we prepared three types of SiNWs with varying lengths. The physical properties of three different SiNWs were determined by analyzing their scanning electron microscopy (SEM) images and are listed in Table 1. The average diameter and density of SiNWs were approximately 130 nm and 120 (per 100 μm^2), respectively (Fig. 1a). This value corresponded to a pitch (inter-NW spacing) of approximately 0.8 μm in an array. The average lengths of the SiNWs were determined as approximately 1.1 ± 0.1 μm (short), 1.9 ± 0.1 μm (medium), and 4.5 ± 0.4 μm (long), resulting in aspect ratios of approximately 1 : 8, 1 : 16, and 1 : 30, respectively (Fig. 1a). Both Si wafers and SiNWs were silanized with (3-aminopropyl)trimethoxysilane (APTMS) for the enhancement of cell adhesions. When stained with carboxyfluorescein diacetate (CFDA), the hMSCs cultured on long SiNWs after 3 days of incubation showed marked morphological changes with elongated shapes and neurite-like structures in the absence of any neural differentiation-inducing reagent (Fig. 1b). Interestingly, these elongated shapes with neurite-like morphological changes were not obvious when short SiNWs were used. Because the morphological changes were the most pronounced with long SiNWs, we focused on characterizing cells on long SiNWs by analyzing the number of extensions (longer than 5 μm), as well as the aspect ratios of the elongated cells, by fitting cells to ellipsoids using ImageJ software (Table 2). As shown in Table 2 and Fig. 1c, the majority of the hMSCs had a higher number of extensions on day 3 than on day 1 although the aspect ratio remained similar.

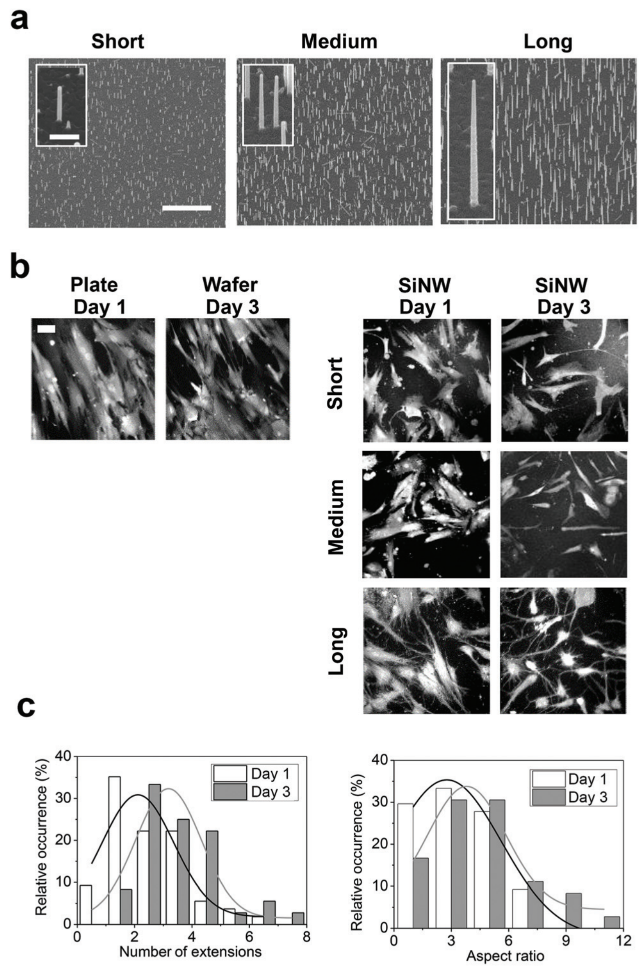

Fig. 1 (a) SEM images of the three different SiNWs, denoted as short, medium, and long according to Table 1. Scale bar, 5 μm. The inset shows the magnified SEM images at a 30 degree angle. Scale bar, 1 μm. (b) Fluorescence images of hMSCs on various surfaces stained with CFDA. The cells were placed on FN-coated glass cover slips, APTMS-treated Si wafers, and three different SiNWs (short, medium, and long) and cultured for 1 and 3 days. For comparison, images of cells on plates and Si wafers cultured for 1 day are also illustrated. Scale bar, 50 μm. (c) Histograms of the number of extensions and the aspect ratio of the cells on long SiNWs. The populations on each day were fit with a single Gaussian distribution.

Table 1 The physical properties of the SiNWs used in this study

	Diameter (bottom surface, μm)	Density (per 100 μm^2)	Length (μm)
Short	0.13 ± 0.01	127 ± 17	1.1 ± 0.1
Medium	0.12 ± 0.01	129 ± 5	1.9 ± 0.1
Long	0.15 ± 0.02	111 ± 8	4.5 ± 0.4

Values are means ± S.D.

Although the physical properties of SiNWs were not exactly same, we consistently observed that HeLa cells significantly decreased membrane trafficking and migration when cells were seeded on a relatively long length of SiNWs (~5.8 μm in length) in the previous study (Fig. S1a†).[18] These etched SiNWs were rather sparsely distributed with lower density.

Table 2 Morphological characteristics of hMSCs cultured on long SiNWs

Incubation day	Aspect ratio	Number of extensions
Day 1	3.3 ± 1.6	2.0 ± 1.4
Day 3	3.0 ± 1.4	4.7 ± 2.5

Values are means ± S.D. The numbers of cells analyzed for both measurements were 54 and 35 for day 1 and day 3, respectively.

When the morphologies of three cell types cultured on these previously prepared SiNWs were examined, HeLa cells were apparently much smaller than those on Si wafers, but there were no apparent shape changes (Fig. S1a†). On the other hand, both hMSCs and human umbilical vein endothelial cells (HUVECs) exhibited dramatic changes in morphology with elongated shapes and neurite-like structures (Fig. S1a†). Furthermore, the elongated morphological changes with neurite-like structures were pronounced as the length of SiNWs increased (Fig. S1b†). These length-dependent morphological changes implied that both hMSCs and HUVECs on SiNWs actively explored the surfaces in an attempt to adjust their morphology while their cell bodies were rather restrained.

Cell motility analysis

Next, we endeavored to measure the cell migration rate using live cell time-lapse imaging. When EGFP expressing hMSCs were cultured on Si wafers, cells migrated freely and showed some directional translational motion as shown in Fig. 2a (see ESI, Movies S1–S4†). On the other hand, hMSCs plated on SiNWs stayed in the same position, while their neurite-like protrusions were continuously stretching out. When we plotted the typical migration traces of 5 different hMSCs on either Si wafers or SiNWs (Fig. 2b), the motility of hMSCs was clearly found to be effectively retarded by SiNWs. Quantification analysis of cell migration showed that hMSCs on Si wafers moved 125 μm on average in 10 h, whereas hMSCs on SiNWs were mostly confined within the 10 μm range (Fig. 2c).

We also confirmed that the HUVEC cell motility on SiNWs is negatively correlated with the length of SiNWs using previously prepared etched SiNWs (Fig. S1c†). In order to form a tube-like structure, the HUVECs must detach their membranes from the surface by degrading matrix proteins and migrate towards each other to enhance cell-to-cell interactions for the formation of new blood vessels.[30] Therefore, patterned, organized cell aggregates randomly located on the Si wafer in Fig. S1c† could be observed only if the cells freely move. However, cells on the fibronectin (FN)-coated Si wafer did not readily move because of the additional process required to degrade the fibronectin matrix, resulting in evenly distributed cells on the surface. Similarly to the FN-coated Si wafer, SiNWs did not produce a tube-like structure of HUVECs. Furthermore, a cell density gradient from the center to the edge of the SiNWs was noticeable in short SiNWs, while such a gradient was barely observed in the cases of medium and long SiNWs

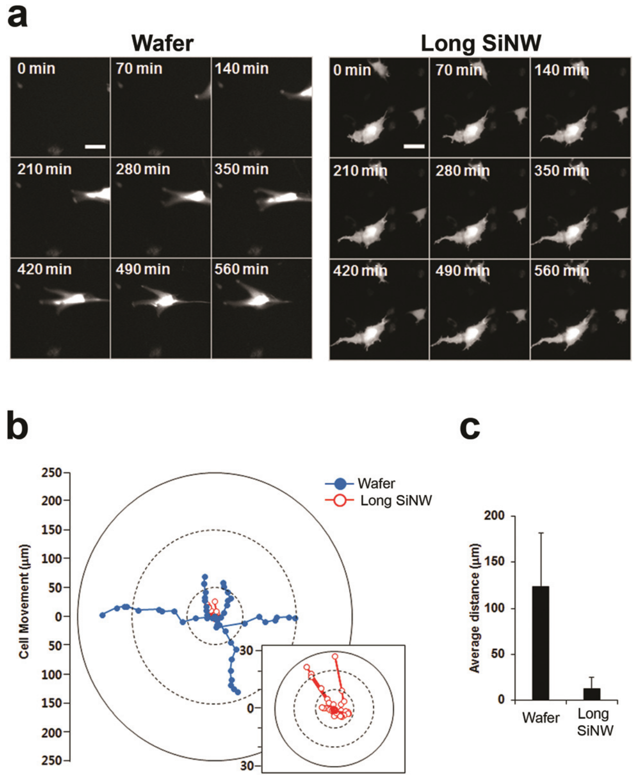

Fig. 2 Cell motility analysis of hMSCs on either Si wafers or SiNWs. (a) The montages from live cell fluorescence imaging for the observation of hMSC migration (see ESI, Movies S1–S4†). (b) Typical movement traces of 5 hMSCs on either Si wafers or SiNWs. (c) Averaged travel distance of hMSCs on either Si wafers or SiNWs. More than 10 cells were tracked from one sample, and two independent experiments were performed.

(Fig. S1c†). Taken together, the cell motility analysis indicated reduced cell mobility on SiNWs, in accordance with other reports.[18,31,32]

Distributions of cytoskeletal actin and focal adhesion

In addition to the changes in cell morphology and migration, we examined the distribution of the actin cytoskeletons and focal adhesions that are important in maintaining the cell shape and for migration on the attached surface. Fig. 3 shows immunofluorescence images of both filamentous actin and vinculin on various surfaces. Strong, fibrillar focal adhesions along the cell axis were colocalized with actin filaments for the cells on FN-coated plates and Si wafers. In contrast, hMSCs on long SiNWs hardly developed such well-organized focal adhesions (Fig. 3), although some dot-like focal complexes were observed in the neurite-like extensions at day 3. When the actin distributions of the cells on long SiNWs were closely inspected, the actin filaments were found to be well organized with neurite-like extensions, whereas small and dot-like actin structures were observed to colocalize notably with the focal complexes (Fig. 3). In general, neurite-like extensions from hMSCs on long SiNWs had relatively well-organized actin filaments and dot-like focal adhesions, while the cell body

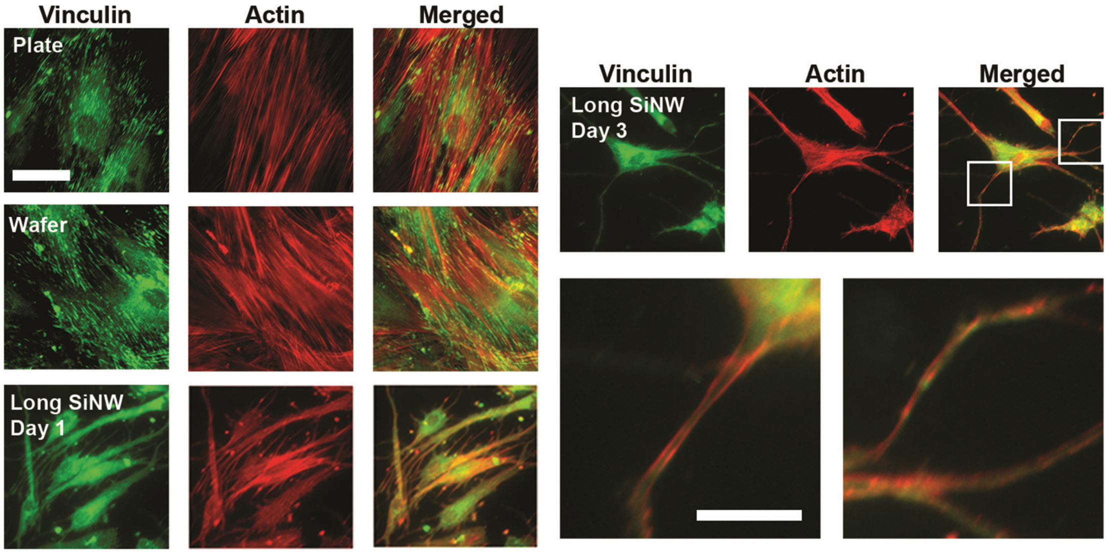

Fig. 3 Immunofluorescence images of hMSCs on various surfaces. The focal adhesion vinculin (green) and cytoskeletal actin filaments (red) were simultaneously visualized by fluorescence microscopy, and the merged images are also presented. Scale bar, 25 μm. Scale bar in the enlarged images, 10 μm.

regions showed some filamentous actin along the cell axis in the background of some of the dot-like actin structures without exhibiting strong focal adhesions. The reduced focal adhesions in the cell body regions in SiNWs were also reported previously with HeLa cells.[18] Given that actin filaments regulate the formation of strong focal adhesions, neurite-like extensions from the cells on long SiNWs likely interacted strongly with the surfaces, where cell body regions did not.

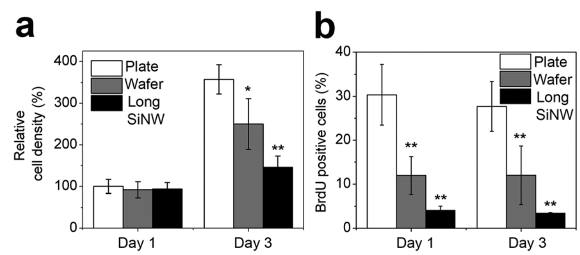

Fig. 4 Cell viability and proliferation of hMSCs on various surfaces. (a) Relative cell viability measured by MTS. The absorbance value of hMSCs on plates on day 1 was set to 1 for comparison. (b) Relative cell proliferation measured by BrdU immunofluorescence. The number of BrdU-positive cells per total number of cells in a given area was calculated for each sample and normalized to the value of hMSCs on plates on each day. The bar represents the mean ± S.D. (*$p < 0.05$, **$p < 0.01$).

Cell viability and proliferation

To evaluate the viability of the hMSCs on long SiNWs, we employed the 3-(4,5-dimethylthiazol-2-yl)-5-(3-carboxymethoxyphenyl)-2-(4-sulfophenyl)-2*H*-tetrazolium (MTS) assay. MTS is a tetrazolium compound that is bioreduced in mitochondria into a colored metabolic product, formazan. Therefore, the amount of formazan produced by cells is proportional to the number of living cells. As shown in Fig. 4a, there was no appreciable difference in the hMSC cell density after a day on various surfaces, indicating that the cells survived and proliferated well in this short period of time. In contrast, the hMSCs on Si wafers and long SiNWs after 3 days of culture had slower cell growth rates, with the rate slightly but significantly lower on Si wafers and approximately 3-fold lower on long SiNWs than on plates. The retarded growth rate of the hMSCs on long SiNWs at day 3 was further supported by counting CFDA-stained cells on long SiNWs (live cells) under a fluorescence microscope (data not shown). Irrespective of such a slowed cell growth, the hMSC cell density on each surface showed higher values at day 3 than at day 1, indicating that the cells were not dying but actually growing slowly during the culture period. We also performed live/dead cell assays based on CFDA/PI staining. As shown in Fig. S2,† the relative percentage of dead cells on long SiNWs (10%) was much less than the decrease in cell density (~43% compared to cells on plates) for long SiNWs. Therefore, the reduced cell density on long SiNWs cannot be ascribed simply to cell death.

The neurite-like extensions, in addition to the observed slower growth rate of hMSCs on long SiNWs, suggested that the cells on long SiNWs may be in a state of neuronal differentiation. Because slowed proliferation and cell cycle arrest is expected upon cell differentiation, we performed 5-bromo-2′-deoxyuridine (BrdU) assays to measure the cellular DNA synthesis rates (S1 phase). BrdU is a pyrimidine analog that is incorporated in place of thymidine into the newly synthesized DNA of the proliferating cells. The magnitude of incorporated BrdU thus indicates the number of S phase cells and the degree of cell proliferation. Specifically, it has been reported that hMSCs exhibit a lower growth capacity upon the induction of cell cycle arrest in the G0/G1 phase.[33] To calculate the relative population of S phase cells, we counted the number of BrdU-positive cells, which was then divided by the total number of cells in each case. As shown in Fig. 4b, the relative population of proliferating cells on long SiNWs was the lowest among all the surfaces, which was consistent with the result from the MTS assay. These observations led us to conclude that the proliferation rate was significantly reduced right after day 1 of cell seeding on long SiNWs, presumably due to cell cycle arrest (Fig. 4b), while the hMSCs were mostly viable and continued to grow (Fig. 4a).

Neural differentiation of hMSCs

Having established the changes in cell morphology, motility, adhesion, viability, and proliferation influenced by long SiNWs, we analyzed the mRNA expression levels of neuron-specific gene markers to confirm the neuronal differentiation of hMSCs. Previous gene expression profile analysis studies revealed enhanced expression of neuronal growth regulator 1 (NEGR1) in response to a neurogenic medium.[34] In addition, upon trans-differentiation of hMSCs into functional neurons validated by measuring neuron specific membrane potentials, both the neurogenic differentiation (NEUROD) and nestin (NES) levels were shown to increase.[22–25] Furthermore, a recent study has illustrated that induction of one specific gene, NEUROD1, is sufficient to trans-differentiate astrocytes to neurons.[35] Accordingly, we detected four neural-lineage-specific marker genes, namely, NEGR1, NEUROD, and NES in addition to a well-known neuronal marker, β-III tubulin (TUBB3), by quantitative real-time PCR. As shown in Fig. 5a, the expression levels of NEGR1, NEUROD, and NES were generally higher in cells on long SiNWs than in those on either plates or Si wafers. Although the level of NEGR1 increased less substantially than those of NEUROD and NES on day 1, it showed a prominent rise on day 3 (Fig. 5a). On the other hand, both NEUROD and NES expressions were strongly upregulated on day 1 and day 3 (Fig. 5a). The levels of TUBB3 that is known to organize along with neuritis were also enhanced (Fig. 5a). The immunostaining data of TUBB3 further indicated that the level of TUBB3 in hMSCs cultured on long SiNWs increased more dramatically than that in hMSCs on Si wafers (Fig. 5b). When hMSCs were cultured on etched SiNWs used in the previous study,[18] the levels of both TUBB3 and NEGR1 also increased with increasing SiNW height (Fig. S1d†). Collectively, the increased expression of TUBB3, NEGR1, NEUROD and NES in the hMSCs on long SiNWs indicated that long SiNWs were capable of inducing more prominent neural differentiation of hMSCs, possibly at an early stage of neurogenesis.

Regarding the differentiation of hMSCs into other lineages, nano-grating structures or aligned nanotube arrays have been reported to promote osteogenic differentiation by stretching cells,[27,36,37] which involves RhoA and ROCK signaling pathways stimulated by cytoskeletal stretching and tension.[38,39] In addition, disruption of the actin assembly by cytochalasin D has been found to interfere with osteogenic differentiation, suggesting an important role of the actin cytoskeleton in osteogenesis. Because we observed reduced focal adhesions in the cell bodies of hMSCs cultured on long SiNWs, we further investigated the effect of SiNWs on the osteogenic differentiation of hMSCs. As shown in Fig. 5a, SiNWs appeared to reduce the expression of an osteogenic gene marker, collagen, type I, alpha 1 (COL1A1), thereby impairing osteogenic differentiation of hMSCs, while runt-related transcription factor 2

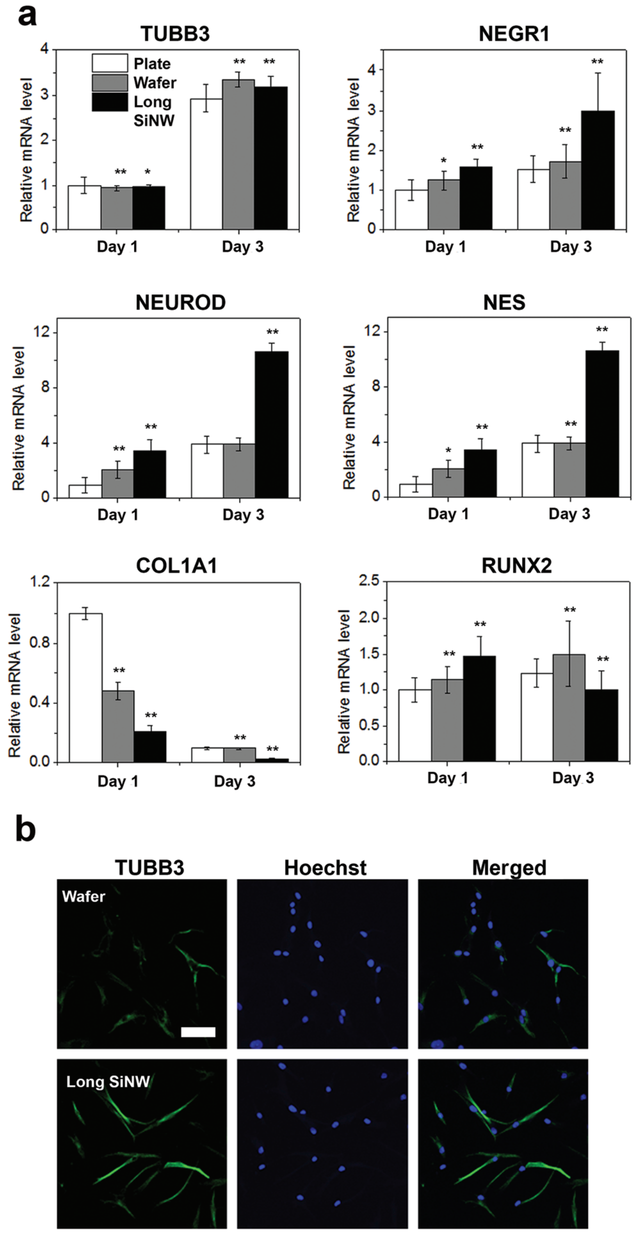

Fig. 5 (a) Real-time PCR analysis of hMSCs for neuronal markers (TUBB3, NEGR1, NEUROD, and NES) and osteoblast markers (COL1A1 and RUNX2). Each mRNA level was normalized to that of GAPDH, and the mRNA level of hMSCs on the culture plate at day 1 was set to 1 for comparison. The bar represents the mean ± S.D. (*$p < 0.05$, **$p < 0.01$). (b) TUBB3 immunofluorescence of hMSCs on either Si wafers or SiNWs (day 3). Both TUBB3 and the nucleus were simultaneously visualized by fluorescence microscopy. Scale bar, 100 μm.

(RUNX2) in hMSCs on long SiNWs increased transiently on day 1 but decreased on day 3. Furthermore, even when hMSCs were cultured in the presence of osteogenic supplements, the cells on long etched SiNWs exhibited significantly reduced expression levels of osteogenic genes, RUNX2 and COL1A1 (Fig. S1d†).

Taken together, our data demonstrated that hMSCs on long SiNWs preferentially differentiate into neuronal lineage cells rather than osteoblasts. Although a few studies with NWs claimed that confined cell spreading or cell aggregation caused by NWs likely accelerated the osteogenic differentiation of stem cells,[14,40] other studies, as well as our data, implied that NWs facilitate neural differentiation.[26–28] Consistent with our observations, a recent study employing well organized, patterned nanopillars with physical properties similar to those of the SiNWs used in this study illustrated the possibility of C3H10T1 cell differentiation toward the neural lineage.[19] Interestingly, the authors also described elongated and polarized morphological changes in hMSCs.[19] Although the elongated shape does not necessarily represent the typical neuron, several studies have demonstrated that hMSCs with elongated shapes also express several markers specific for a neuronal lineage.[16,41–43]

Our observations of cell behaviors on SiNWs have thus led to the speculation that cells stuck on long SiNWs by impalement are incapable of evacuating from the unfavorable surface but might actively explore more favorable physical environments *via* outgrowing neurite-like extensions, resulting in the reprogramming of the hMSCs into a neuronal cell lineage. This phenomenon is supported by previous reports, showing that SiNWs could facilitate neurite outgrowth from the neuronal cell body which was maintained in a stationary state.[19,44]

Conclusions

Based on our collective understanding of cell adhesion and morphological changes in mammalian cells on SiNWs, we demonstrated that SiNWs could direct the fate of hMSCs into a neural lineage. The most pronounced morphological change associated with the neurite-like extensions was observed when hMSCs were cultured on long SiNWs. Live cell imaging clearly demonstrated a cell motility decrease, and immunofluorescence imaging showed well-developed actin filaments with dot-like focal adhesions in the neurite-like extensions, suggesting strong interactions of hMSCs with the surface. The slower growth rate of hMSCs on long SiNWs, along with a constantly low proliferation rate, indicated cell cycle arrest for proper cell differentiation, and changes in the mRNA levels of various neural markers implied that hMSCs were possibly at an early stage of neurogenesis. Overall, we believe that the inhibition of cell migration on long SiNWs as well as the enhanced surface exploration by neurite-like extensions likely facilitated the observed morphological changes, resulting in a shifted fate of the hMSCs into the neuronal lineage even in the absence of any inducing reagent.

Experimental

Cell culture

HeLa cells (Korean Cell Line Bank, Korea) were grown in Dulbecco's modified Eagle's medium (DMEM, Gibco, USA) supplemented with 10% fetal bovine serum (Gibco, USA) and 1% penicillin/streptomycin (Gibco, USA) at 37 °C with 5% CO_2. hMSCs were purchased from Lonza (PT-2501, USA) and maintained in hMSC growth medium with appropriate supplements (PT-3001, Lonza, USA) at 37 °C with 5% CO_2. HUVECs were obtained from Life Technologies (USA) and grown in M200 media with an LSGS supplement (Gibco, USA). Experiments with HUVECs were performed with fewer than 10 cell passages.

Preparation of SiNWs

Vertically aligned SiNWs were synthesized on an intrinsic Si(111) substrate deposited with a 5 nm-thick Au catalyst layer according to the vapor–liquid–solid process. Silane (SiH_4) gas, a precursor, and H_2, a dilution gas, were introduced into a reactor at 550 °C for 9 h under high-vacuum conditions to facilitate the growth of the SiNWs.[45,46]

Surface modification of SiNWs

For proper cell attachment, we functionalized both the SiNWs and Si wafers with APTMS (Sigma-Aldrich, USA) to cover the surface with positively charged amine groups. The hydroxyl groups on the surface were exposed by treating the SiNWs and Si wafers with oxygen plasma for 10 min. Using acetic acid (5% v/v) as a catalyst, silanization was carried out at room temperature for 30 min with APTMS in methanol. The treated substrates were washed with methanol and water and then dried with nitrogen gas. To avoid any contamination, the substrates were further rinsed thrice with Dulbecco's phosphate-buffered saline (PBS) in a tissue culture hood before cell seeding.

Live and dead cell staining with CFDA and propidium iodide (PI)

Approximately 5×10^2 of hMSCs were seeded on culture plates, Si wafers, or SiNWs (the same area of 0.5×0.5 cm^2) and stained with the mixture of 1 μM CFDA (Sigma-Aldrich, USA) and 1 μM PI (Sigma-Aldrich, USA) at days 1 and 3. The CFDA solution was added to the medium containing the cell-plated substrate, followed by incubation for 10 min. The cell-plated substrate was washed twice with PBS before imaging. The stained cells were visualized by fluorescence imaging performed at 528 ± 19 nm (excitation at 490 ± 10 nm) using a fluorescence microscope (Deltavision, Applied Precision).

Live cell time-lapse imaging and motility analysis

hMSCs transiently expressing cytoplasmic EGFP for fluorescence detection were seeded on either Si wafers or SiNWs, and cultured overnight for proper attachment. For live cell imaging, a Chamlide live cell imaging system (CU105 with a Chamlide TC chamber, Live Cell Instrument, Korea) was used to control temperature, humidity and CO_2 gas (37 °C, 40%

humidity, 5% CO_2). Fluorescence images of transfected cells were obtained using a fluorescence microscope (ECLIPSE Ti-E, Nikon, Japan). For EGFP excitation and emission, 490 ± 10 nm and 528 ± 19 nm filters were used, respectively. The fluorescence was imaged every 10 min for 10 h on an EMCCD (iXon3, Andor, USA), and more than 10 images for each sample were collected. Two independent experiments were performed. For cell motility analysis, cells were manually tracked by tracking their center of mass using thresholded images, and their average velocity was calculated.

Immunofluorescence imaging

hMSCs on various substrates were fixed with 4% paraformaldehyde in PBS and then permeabilized with 0.5% Triton X-100. The cells were washed with PBS and then incubated with an anti-vinculin primary antibody (Sigma-Aldrich, USA). The anti-vinculin antibody was detected using an Alexa-488-conjugated, isotype-specific secondary antibody to IgG (Abcam, USA). TRITC-conjugated phalloidin (Sigma-Aldrich, USA) was added for F-actin visualization. Labeled vinculin was visualized with excitation at 490 ± 10 nm and fluorescence at 528 ± 19 nm, and F-actin was detected with excitation at 555 ± 14 nm and fluorescence at 617 ± 36 nm using a fluorescence microscope (Deltavision, Applied Precision). For TUBB3 staining, anti-TUBB3 (Abcam, USA) was added and visualized using an Alexa 488-conjugated secondary antibody to IgG. The nucleus was stained with Hoechst (Invitrogen, USA).

Cell viability and proliferation assay

The cell viability was determined using the CellTiter 96 Aqueous One Solution Cell Proliferation assay (MTS assay, Promega, USA) according to the protocols provided by the manufacturer. Briefly, hMSCs on various substrates at days 1 and 3 were placed in 48-well plates with 20% MTS solution in fresh growth medium and were incubated for 3 h at 37 °C. The change in absorbance at 490 nm was measured using a spectrophotometric plate reader. The cell proliferation was assessed by using a BrdU Cell Proliferation Assay kit (Cell Signaling, USA) with some modifications. hMSCs on various substrates on specified days were incubated with the BrdU solution overnight at 37 °C. BrdU-incorporated cells were then fixed with 4% paraformaldehyde in PBS and permeabilized with 0.5% Triton X-100. The DNA was further denatured with 2 N HCl for 30 min at 37 °C and then neutralized with 0.1 M sodium borate buffer (pH 8.5) for 10 min. The treated cells were washed with PBS containing 0.1% Tween 20 (PBST) and were incubated overnight at 4 °C with an anti-BrdU antibody in PBST containing 5% bovine serum albumin (BSA). The cells were washed thrice with PBST and treated with the Alexa-488-labeled secondary antibody (Abcam, USA) in PBST containing 5% BSA and PI. The stained cells were observed under a fluorescence microscope with an excitation wavelength of 490 ± 10 nm and fluorescence at 528 ± 19 nm for BrdU detection and an excitation wavelength of 555 ± 14 nm and an emission wavelength of 617 ± 36 nm for PI detection. The cell proliferation rates were estimated by calculating the ratio of the number of BrdU-positive cells to the total number of cells counted by PI staining. The total number of cells analyzed for the BrdU assay were as follows: 357, 359 and 242 cells for plates, wafers and SiNWs on day 1; 534, 931 and 748 cells for plates, wafers and SiNWs on day 3, respectively. The cell proliferation rate of hMSCs on plates for each day was set to 1 for comparison.

Neuronal differentiation and real-time PCR

For neuronal differentiation, approximately 5 × 10^2 hMSCs were seeded on culture plates, Si wafers, or SiNWs (the same area of 0.5 × 0.5 cm^2), and the cells were maintained in the hMSC growth medium with appropriate supplementation. We used 8–12 replicate samples for the extraction of mRNA, and the total cellular mRNA from the cells at days 1 and 3 was isolated using the RNeasy mini kit (Qiagen, USA) according to the manufacturer's instructions. The total RNA (approximately 0.5 μg) was reverse-transcribed using the TOPscript cDNA synthesis kit (Enzynomics, Korea), and 1 μL of cDNA was analyzed by real-time PCR using the Power SYBR Green kit (Applied Biosystems, USA) on a StepOne™ instrument (Applied Biosystems). The primer sequences used in this study are described in Table S1.† To amplify and quantify the mRNAs of osteoblast markers (COL1A1 and RUNX2), neuronal markers (NES, NEUROD, TUBB3, and NEGR1), and the GAPDH control, the following conditions were used: pre-incubation at 46 °C for 30 min, an initial melt at 95 °C for 10 min, and 40 cycles of amplification (95 °C for 15 s, 60 °C for 60 s) with 5 μM of each primer. Each mRNA level was normalized to that of GAPDH, and the mRNA level of hMSCs on the culture plate was set to 1 for comparison. The mRNA expression was compared according to the $2^{-\Delta\Delta CT}$ method.

Data analysis and statistics

The data represent three independent experiments. The results are presented as the means ± standard deviation (S.D.). Statistical analyses were performed with Student's *t*-test using SigmaPlot 8.0 software.

Acknowledgements

This work was supported by the Multi-omics Research Program funded by the Korean Ministry of Science, ICT and Future Planning, and by the KIST grant (2E25270).

References

1 K. Ghosh and D. E. Ingber, *Adv. Drug Delivery Rev.*, 2007, **59**, 1306.
2 M. Peran, M. A. Garcia, E. Lopez-Ruiz, M. Bustamante, G. Jimenez, R. Madeddu and J. A. Marchal, *Int. J. Mol. Sci.*, 2012, **13**, 3847.
3 I. Ilie, R. Ilie, T. Mocan, D. Bartos and L. Mocan, *Int. J. Nanomedicine*, 2012, **7**, 2211.

4 J. Y. Hwang, U. S. Shin, W. C. Jang, J. K. Hyun, I. B. Wall and H. W. Kim, *Nanoscale*, 2013, **5**, 487.
5 G. W. Wang, Y. N. Lu, L. P. Wang, H. J. Wang and J. Y. Wang, *J. Nanosci. Nanotechnol.*, 2014, **14**, 596.
6 W. Kim, J. K. Ng, M. E. Kunitake, B. R. Conklin and P. Yang, *J. Am. Chem. Soc.*, 2007, **129**, 7228.
7 W. Hallstrom, T. Martensson, C. Prinz, P. Gustavsson, L. Montelius, L. Samuelson and M. Kanje, *Nano Lett.*, 2007, **7**, 2960.
8 Z. Li, J. Song, G. Mantini, M. Y. Lu, H. Fang, C. Falconi, L. J. Chen and Z. L. Wang, *Nano Lett.*, 2009, **9**, 3575.
9 A. K. Shalek, J. T. Robinson, E. S. Karp, J. S. Lee, D. R. Ahn, M. H. Yoon, A. Sutton, M. Jorgolli, R. S. Gertner, T. S. Gujral, G. MacBeath, E. G. Yang and H. Park, *Proc. Natl. Acad. Sci. U. S. A.*, 2010, **107**, 1870.
10 C. Xie, L. Hanson, Y. Cui and B. Cui, *Proc. Natl. Acad. Sci. U. S. A.*, 2011, **108**, 3894.
11 G. S. Park, H. Kwon, D. W. Kwak, S. Y. Park, M. Kim, J. H. Lee, H. Han, S. Heo, X. S. Li, J. H. Lee, Y. H. Kim, J. G. Lee, W. Yang, H. Y. Cho, S. K. Kim and K. Kim, *Nano Lett.*, 2012, **12**, 1638.
12 B. K. Teo, S. Ankam, L. Y. Chan and E. K. Yim, *Methods Cell Biol.*, 2010, **98**, 241.
13 K. S. Brammer, C. Choi, C. J. Frandsen, S. Oh and S. Jin, *Acta Biomater.*, 2011, **7**, 683.
14 S. W. Kuo, H. I. Lin, J. H. Ho, Y. R. Shih, H. F. Chen, T. J. Yen and O. K. Lee, *Biomaterials*, 2012, **33**, 5013.
15 D. Khang, J. Choi, Y. M. Im, Y. J. Kim, J. H. Jang, S. S. Kang, T. H. Nam, J. Song and J. W. Park, *Biomaterials*, 2012, **33**, 5997.
16 B. K. Teo, S. T. Wong, C. K. Lim, T. Y. Kung, C. H. Yap, Y. Ramagopal, L. H. Romer and E. K. Yim, *ACS Nano*, 2013, **7**, 4785.
17 K. Yang, K. Jung, E. Ko, J. Kim, K. I. Park, J. Kim and S. W. Cho, *ACS Appl. Mater. Interfaces*, 2013, **5**, 10529.
18 S. Y. Kim and E. G. Yang, *Nanotechnology*, 2013, **24**, 455704.
19 M. A. Bucaro, Y. Vasquez, B. D. Hatton and J. Aizenberg, *ACS Nano*, 2012, **6**, 6222.
20 C. Krabbe, J. Zimmer and M. Meyer, *APMIS*, 2005, **113**, 831.
21 A. Uccelli, A. Laroni and M. S. Freedman, *Lancet Neurol.*, 2011, **10**, 649.
22 M. Dezawa, H. Kanno, M. Hoshino, H. Cho, N. Matsumoto, Y. Itokazu, N. Tajima, H. Yamada, H. Sawada, H. Ishikawa, T. Mimura, M. Kitada, Y. Suzuki and C. Ide, *J. Clin. Invest.*, 2004, **113**, 1701.
23 M. Hayase, M. Kitada, S. Wakao, Y. Itokazu, K. Nozaki, N. Hashimoto, Y. Takagi and M. Dezawa, *J. Cereb. Blood Flow Metab.*, 2009, **29**, 1409.
24 H. Gu, Z. Yue, W. S. Leong, B. Nugraha and L. P. Tan, *Regen. Med.*, 2010, **5**, 245.
25 A. Hermann, R. Gastl, S. Liebau, M. O. Popa, J. Fiedler, B. O. Boehm, M. Maisel, H. Lerche, J. Schwarz, R. Brenner and A. Storch, *J. Cell Sci.*, 2004, **117**, 4411.
26 A. J. Engler, S. Sen, H. L. Sweeney and D. E. Discher, *Cell*, 2006, **126**, 677.
27 S. Oh, K. S. Brammer, Y. S. Li, D. Teng, A. J. Engler, S. Chien and S. Jin, *Proc. Natl. Acad. Sci. U. S. A.*, 2009, **106**, 2130.
28 K. A. Kilian, B. Bugarija, B. T. Lahn and M. Mrksich, *Proc. Natl. Acad. Sci. U. S. A.*, 2010, **107**, 4872.
29 Y. S. Chen and G. H. Hsiue, *Biomaterials*, 2013, **34**, 4936.
30 I. Arnaoutova, J. George, H. K. Kleinman and G. Benton, *Angiogenesis*, 2009, **12**, 267.
31 H. Persson, C. Kobler, K. Molhave, L. Samuelson, J. O. Tegenfeldt, S. Oredsson and C. N. Prinz, *Small*, 2013, **9**, 4006.
32 C. Xie, L. Hanson, W. Xie, Z. Lin, B. Cui and Y. Cui, *Nano Lett.*, 2010, **10**, 4020.
33 H. E. Park, D. Kim, H. S. Koh, S. Cho, J. S. Sung and J. Y. Kim, *J. Biomed. Biotechnol.*, 2011, **2011**, 485173.
34 T. Tondreau, M. Dejeneffe, N. Meuleman, B. Stamatopoulos, A. Delforge, P. Martiat, D. Bron and L. Lagneaux, *BMC Genomics*, 2008, **9**, 166.
35 Z. Guo, L. Zhang, Z. Wu, Y. Chen, F. Wang and G. Chen, *Cell Stem Cell*, 2014, **14**, 188.
36 S. Watari, K. Hayashi, J. A. Wood, P. Russell, P. F. Nealey, C. J. Murphy and D. C. Genetos, *Biomaterials*, 2012, **33**, 128.
37 S. Namgung, K. Y. Baik, J. Park and S. Hong, *ACS Nano*, 2011, **5**, 7383.
38 R. McBeath, D. M. Pirone, C. M. Nelson, K. Bhadriraju and C. S. Chen, *Dev. Cell*, 2004, **6**, 483.
39 E. J. Arnsdorf, P. Tummala, R. Y. Kwon and C. R. Jacobs, *J. Cell Sci.*, 2009, **122**, 546.
40 S. Bechara, L. Wadman and K. C. Popat, *Acta Biomater.*, 2011, **7**, 2892.
41 E. K. Yim, S. W. Pang and K. W. Leong, *Exp. Cell Res.*, 2007, **313**, 1820.
42 S. Y. Park, B. S. Kang and S. Hong, *Nanomedicine*, 2013, **8**, 715.
43 J. Yoo, M. Noh, H. Kim, N. L. Jeon, B. S. Kim and J. Kim, *Biomaterials*, 2015, **45**, 36.
44 G. Piret, M. T. Perez and C. N. Prinz, *Biomaterials*, 2013, **34**, 875.
45 J. Westwater, D. P. Gosain, S. Tomiya, S. Usui and H. Ruda, *J. Vac. Sci. Technol., B*, 1997, **15**, 554.
46 K. Y. Lee, I. Kim, S. E. Kim, D. W. Jeong, J. J. Kim, H. Rhim, J. P. Ahn, S. H. Park and H. J. Choi, *Nanoscale Res. Lett.*, 2014, **9**, 56.